Is the Prion Domain of Soluble Ure2p Unstructured?

Michael M. Pierce,‡ Ulrich Baxa,‡,§ Alasdair C. Steven,§ Ad Bax,⊥ and Reed B. Wickner*,‡

Laboratory of Biochemistry and Genetics, National Institute of Diabetes and Digestive and Kidney Diseases, Laboratory of Structural Biology, National Institute of Arthritis and Musculoskeletal and Skin Diseases, and Laboratory of Chemical Physics, National Institute of Diabetes and Digestive and Kidney Diseases, National Institutes of Health, Bethesda, Maryland 20892-0830

ABSTRACT: The [URE3] prion is a self-propagating amyloid form of the Ure2 protein of *Saccharomyces cerevisiae*. Deletions in the C-terminal nitrogen regulation domain of Ure2p increase the frequency with which the N-terminal prion domain polymerizes into the prion form, suggesting that the C-terminus stabilizes the prion domain or that the structured C-terminal region sterically impairs amyloid formation. We find by in vivo two-hybrid analysis no evidence of interaction of prion domain and C-terminal domain. Furthermore, surface plasmon resonance spectrometry shows no evidence of interaction of prion domain and C-terminal domain, and cleavage at a specific site between the domains frees the two fragments. Our NMR analysis indicates that most residues of the prion domain are in fact disordered in the soluble form of Ure2p. Deleting the tether holding the C-terminal structured region to the amyloid core does not impair prion formation, arguing against steric impairment of amyloid formation. These results suggest that the N-terminal prion domain is unstructured in the soluble protein and does not have a specific interaction with the C-terminus.

The nonchromosomal genes [URE3] and [PSI] of *Saccharomyces cerevisiae* are infectious proteins (prions) of Ure2p and Sup35p, respectively (*1*). Similarly, the [Het-s] nonchromosomal gene is a prion of the HET-s protein of the filamentous fungus *Podospora anserina* (*2*). Each of these systems is based on the formation of a self-propagating amyloid form of the respective protein (*3–9*, reviewed in ref *10*). In each protein, a limited part of the molecule comprises a domain that is necessary and sufficient for the prion properties of the molecule (*11–14*). In the case of Ure2p and the HET-s protein, the prion domain roughly corresponds to the amyloid core of the molecule (*14, 15*). The maximal Ure2p prion domain comprises residues 1−89, but residues 1−65 are sufficient for high-efficiency prion induction in vivo (*12*) and transmission of [URE3] without the C-terminal domain (*16*) and constitute the amyloid core that is resistant to high levels of proteinase K (*15*).

For Ure2p and Sup35p, deletion of regions outside the prion domain results in marked elevation of the prion-inducing activity of the prion domain itself (*12, 17*). Deletions or mutations outside the HET-s protein prion domain have likewise been shown to dramatically affect prion generation in vivo and amyloid formation in vitro (*14, 18*). This has led to the suggestion that the prion domain interacts with the remainder of the molecule and that this interaction stabilizes the prion domain and prevents its conversion to the prion form (*12, 14, 17*). An earlier two-hybrid analysis of parts of Ure2p was complicated by

activation activity of the C-terminal domain alone (*19*), apparently by recruiting Gln3p (*20*). Nonetheless, the results showed an interaction of Ure2p$^{1-152}$ with Ure2p$^{152-354}$ (*19*). This result is consistent with interaction of the prion domain (Ure2p$^{1-89}$) with the C-terminal fragment (Ure2p$^{95-354}$), but might be an interaction of two parts of the C-terminal domain.

The Ure2p prion domain has been shown to be relatively protease-sensitive in the soluble form (*15, 21*), and denaturation studies showed no stabilization of the molecule attributable to the prion domain (*21–23*). These results are inconsistent with a strong structure of this part of the molecule but do not imply the absence of structure.

Ure2p homologues from a number of yeasts and fungi have highly conserved C-terminal domains and could carry out the nitrogen regulation function of Ure2p of *S. cerevisiae* (*24*). The N-terminal domains were not as highly conserved, though most were rich in asparagine and glutamine residues. Within the N-terminal domain was a region, approximately residues 10−39, that was quite well conserved among *S. cerevisiae, Ashbya gossypii, Candida kefyr, Candida glabrata,* and *Candida lactis* (*24*). It was suggested that this conserved region might interact with the C-terminal domain, particularly since overexpression of this region inhibited the nitrogen regulation function of Ure2p in a [ure-o] strain (*24*).

With several lines of evidence suggesting interaction of the Ure2p N-terminal prion domain and its C-terminal functional nitrogen regulation domain, we undertook several direct approaches to examine this issue. In each case, we find no evidence for such an interaction.

MATERIALS AND METHODS

Plasmid Construction. Fragments of *URE2* corresponding to the N-terminal prion domain (*URE2* 1−80), the C-terminal

* Contact information: Bldg. 8, Room 225, NIH, 8 Center Drive MSC 0830, Bethesda, MD 20892-0830. Phone: 301-496-3452. Fax: 301-402-0240. E-mail: wickner@helix.nih.gov.
‡ Laboratory of Biochemistry and Genetics, NIDDK.
§ Laboratory of Structural Biology, NIAMS.
⊥ Laboratory of Chemical Physics, NIDDK.

nitrogen regulation domain (*URE2* 81−354), or the full-length open reading frame (*URE2* 1−354) were cloned as in frame fusions to either the Gal4p activation domain or Gal4p binding domain vectors pGADT7 and pGBKT7 (Clontech). Activation and binding domain fusions were constructed by PCR amplification of *URE2* 1−80, *URE2* 81−354, and *URE2* 1−354 with primers 1−80Eco_f (5′-tacgtagaattccatgatgaataacaacggcaacc-3′), 1−80Bam_r (5′-acctggggatcctcaggtattcttgatattattctcgttatc-3′), 81−354Eco_f (5′-tactgagaattccttagaacaacatcgacaacaac-3′), and 81−354Bam-R (5′-accttgggatcctcattccaccacgcaatgccttg-3′) using plasmid pMP45 (2 *μ*m *HIS*3 P$_{ADH1}$ *URE2*) as template. Primers 1−80Eco_f and 1−80Bam-r were used to amplify *URE2* 1−80. Oligonucleotides 81−354Eco_f and 81−354Bam-r were used to amplify *URE2* 81−354. Oligonucleotides 1−80Eco_f and 81−354Bam_r were used to amplify the full-length *URE2* construct, *URE2* 1−354. *Eco*RI and *Bam*HI restriction sites, underlined in the above primer sequences, were added to the *URE2* constructs during the PCR amplification reactions. The PCR constructs were cut with *Eco*RI and *Bam*HI and ligated into *Eco*RI/*Bam*HI cut pGADT7 or pGBKT7 to generate the Gal4p-*URE2* plasmids.

Expression of Ure2p or fragments thereof in *Escherichia coli* for NMR[1] studies was from pKT41-1 (*15*), pKT51 (His6-DDDDK-Ure2p$^{66−354}$, gift of Kimberly Taylor), and pUB9, the latter constructed by amplification of the required region of the URE2 gene using polymerase chain reaction with primers 5′-tatactcgagtcattcaccacgcaatgcc-3′ and 5′-attacatatgcatcaccatcaccatcacagtcacgtggagtattcc-3′. The PCR product was cloned into pET17b using the *Nde*I and *Xho*I restriction sites.

The construction of full-length Ure2p containing a factor Xa proteolytic site was performed as follows. First, *URE2* was cloned into the pFLAG (Kodak) *E. coli* expression vector by cutting pMP20 (CEN LEU2 P$_{Gal1}$*URE2*) with *Not*I and *Xho*I and ligating the insert into *Not*I/*Xho*I digested pKT 55 (*15*) generating plasmid pMP56. The AGA codons at positions 253 and 254 were changed to CGT using the QuikChange site-directed mutagenesis kit (Stratagene) with primers KT044 (5′-cggatgaggttcgtcgtgtttacggtgtag-3′) and KT045 (5′-ctacaccgtaaacacgacgaacctcatccg-3′) generating plasmid pMP62. The AGA to CGT mutations have previously been shown to improve expression of Ure2p in *E. coli* (*24a*). An insertion of two amino acid residues (IE) following amino acid 63 was constructed using the QuikChange mutagenesis kit and primers URE2_65FXf (5′-caaaacaataacagcatcgaaggccgcaatggtagc-3′) and URE2_65FXr (5′-gctaccattgcggccttcgatgctgttattgttttg-3′) yielding plasmid pMP77. This plasmid encodes a His$_6$-tagged Ure2p (Ure2p65FX) with a factor Xa proteolytic site (IEGR), which is cleaved by the factor Xa protease following Arg65.

*URE2*Δ71−95, lacking the tether region, was constructed by PCR amplification from a *URE2* plasmid template with oligos 143 (5′-acaataacagcggccgcaatggtagccaaaatcacgtggagtaggccaga-3′) and 134 (5′-caaattcggggggccctatgtt-3′), digestion with *Apa*I and *Not*I, and insertion into p588 cut with the same enzymes forming p1033. To integrate *URE2*Δ71−95, *URE2*Δ71−95 as a *Bam*HI/*Xba*I fragment from p1033 was ligated into *Bam*HI/*Xba*I digested p1013 (*CEN LEU2*

P$_{URE2}$) generating p1038. Next, 50 *μ*g of p1038 was digested with *Nhe*I and *Xba*I and the 3.4 kb insert containing the *URE2* promoter and *URE2*Δ71−95 open reading frame was gel-purified. Ten micrograms of the gel purified *Nhe*I/*Xba*I fragment was transformed into strain YMT1 (*MAT*α *ura2 leu2 ure2::G418* P$_{DAL5}$*CAN1*). Integrants were selected on SC-Arg + canavanine (66 *μ*g/mL) and tested for sensitivity to the antibiotic G418. The integration of *URE2*Δ71−95 was confirmed by colony PCR analysis using primer pairs to determine both the presence of the *URE2*Δ71−95 construct and the absence of the G418 selectable marker present in the parent strain YMT1.

Protein Expression and Purification. Expression and purification of Ure2p-65FX was performed as previously described (*15*). Protein was purified in one step on a nickel-NTA Superflow column (Qiagen). Following elution from the column, the protein was immediately frozen in liquid nitrogen and stored at −80 °C.

Expression of ^{15}N-labeled proteins was from the following vectors: Ure2p from pKT41-1, Ure2p$^{66−354}$ from pKT51, Ure2p$^{95−354}$ from pUB9. *E. coli* BL21(DE3) transformed with the respective plasmid was grown at 37 °C in M9-medium supplemented with [15]NH$_4$Cl and 50 *μ*g/mL ampicillin to an OD ≈ 1, and then IPTG to 1 mM was added. The cells were incubated for another 4 h and then harvested by centrifugation, taken up in 50 mM NaPO$_4$, 300 mM NaCl, pH 8.0 (buffer A), and lysed by high pressure. Extracts were then cleared by high-speed centrifugation at 40 000*g* for 1 h, and supernatants were loaded onto a NiNTA column, washed with 10 column volumes of 20 mM imidazole in buffer A, and eluted in one peak with 250 mM imidazole in buffer A. Exact sequences for the three constructs are as follows: KT41-1, MHHHHHHMYPRGN−Ure2p1−354; KT51, MH-HHHHHDDDDK−Ure2p66−354; UB9, MHHHHHH−Ure2p95−354.

Purified proteins were concentrated in Centricon (Millipore) and dialyzed against the NMR buffer (20 mM NaPO$_4$, 100 mM NaCl, pH 7.0) overnight. Any aggregated protein was removed by centrifugation, and 5% (v/v) D$_2$O was added before measurement to have a frequency lock signal for the NMR instrument.

For surface plasmon resonance, His$_6$Ure2$^{81−354}$ was purified using pKT50 (gift from Kimberly Taylor) as previously described (*15*) by nickel-NTA chromatography and immediately frozen in liquid nitrogen and stored at −80 °C. The prion domain was Ure2p$^{1−89}$ with Gln89 changed to cysteine to facilitate immobilization to the biosensor (gift of Todd Cassese). Ure2p$^{1−89}$Cys was purified under denaturing conditions to prevent aggregation. Briefly, *E. coli* BL21 in 1 L of LB media containing 0.1 mg/mL ampicillin was grown to OD$_{550}$ = 1 and induced by the addition of IPTG to 1 mM. The cultures were grown for an additional 4 h before harvesting. Five grams of cells was suspended in 30 mL of buffer A (0.1 M sodium phosphate, 0.01 M Tris, 6 M guanidine hydrochloride, pH 8.0) and lysed by passing two times through a French pressure cell. The cell lysate was centrifuged at 12 000 rpm for 15 min to remove insoluble material. Next, 3 mL of nickel-NTA resin (Qiagen) equilibrated in buffer A was added to the supernatant and gently mixed for 30 min at 25 °C. The slurry was centrifuged for 1 min at 500 rpm and washed with 20 mL of buffer A, 20

---

[1] Abbreviations: NMR, nuclear magnetic resonance; HSQC, heteronuclear single quantum coherence; SPR, surface plasmon resonance.

mL of buffer B (0.1 M sodium phosphate, 0.01 M Tris, 8 M urea, pH 8.0), and 20 mL of buffer C (0.1 M sodium phosphate, 0.01 M Tris, 8 M urea, pH 6.3). Protein was eluted in two fractions with 6 mL of buffer D (0.1 M sodium phosphate, 0.01 M Tris, 8 M urea, pH 5.9) and 6 mL of buffer E (0.1 M sodium phosphate, 0.01 M Tris, 8 M urea, pH 4.5). The majority of $Ure2p^{1-89}Cys$ was present in the second fraction. Purified $Ure2p^{1-89}Cys$ was dialyzed overnight in water. Following this step, most of the protein consisted of an insoluble aggregate. The insoluble material was recovered, washed two times with water, and dried in a speed-vac centrifuge. For the SPR experiments, $Ure2p^{1-89}Cys$ was initially solubilized in 8 M GdnHCl. Prior to immobilization to the biosensor, the GdnHCl was adjusted to 6 M.

Surface Plasmon Resonance Biosensing. Biosensor experiments were conducted with a Biacore X instrument (Biacore, Piscataway, NJ). As a sensor surface, C1 chips (Biacore, Piscataway, NJ) were used, which have a carboxylated surface but not the usual flexible Dextran immobilization matrix. Immobilization followed standard protocols for covalent thioester coupling (25, 26). In brief, after cleaning the chip surface by rinsing with low- and high-pH buffers, the carboxyl groups were activated for 7 min with a mixture of *N*-ethyl-*N'*-(3-dimethylaminopropyl)-carbodiimide hydrochloride and *N*-hydroxy-succinimide; ethylenediamine was attached by 10 min exposure at 1 M concentration, pH 6.0, followed by a 20 min incubation with sulfosuccinimidyl-4-(*N*-maleimidomethyl)cyclohexane-1-carboxylate (Pierce, Rockford, IL) dissolved in PBS at 2 mg/mL. The prion domain of Ure2 (residues 1−89) expressed with a C-terminal cysteine was cross-linked to the surface under denaturing conditions at 1 mg/mL in 6 M guanidine HCl, pH 8.5, leading to a signal increase of 800 response units (RU). The surface was deactivated for 2 min with 0.1 M NaOH and rinsed with the running buffer for the binding experiments, 10 mM HEPES, pH 7.4, 150 mM NaCl, 3 mM EDTA, and 0.005% Tween 20. The surface in a second flow cell was treated identically but without exposure to Ure2 to serve as a chemically similar reference to approximate the signals from nonspecific binding and buffer refractive index. After binding experiments, the surface was regenerated with 6 M guanidine HCl. The biosensor experiments were conducted at a temperature of 25 and 13 °C.

NMR Measurement. HSQC (heteronuclear single quantum coherence) NMR spectra were recorded with the standard gradient- and sensitivity-enhanced pulse sequence (27). All spectra result from addition of two sequentially recorded data sets, where comparison between the individual data sets was used to monitor the potential loss of signal resulting from any sample precipitation or fibrillization during the NMR measurements. NMR measurements were carried out at 20 (Ure2p) and 25 °C ($Ure2p^{66-354}$; $Ure2p^{95-354}$) on a Bruker DRX-600 NMR spectrometer operating at 14.1 T and equipped with a cryogenically cooled triple resonance probe head. The buffer for all proteins was 20 mM $NaPO_4$, 100 mM NaCl, pH 7.0. Since NMR signals are linear with protein concentration, it was possible, despite the differences in concentration in the three measurements, to roughly scale the spectra to each other (Figure 3). The NMR spectrum of full-length Ure2p (0.023 mM) resulted from 224 transients per complex t_1 increment for a total measuring time of 15 h.

Similarly, spectra recorded for $Ure2p^{66-354}$ (0.49 mM) and $Ure2p^{95-354}$ (0.021 mM) resulted from 16 ($Ure2p^{66-354}$) and 64 ($Ure2p^{95-354}$) transients per t_1 increment for total measuring times of 1.1 ($Ure2p^{66-354}$) and 4.3 h ($Ure2p^{95-354}$). NMR spectra were recorded as data matrices of 150×1024 complex data points and apodized with squared 90°-shifted sine bell windows prior to zero filling and Fourier transformation to yield a final digital resolution of 4.0 (^{15}N) and 4.2 Hz (^1H). All spectra were processed and analyzed with the NMRPipe software system (28). The very limited solubility and sample stability prohibited sequential backbone assignment of the protein by standard 3D triple resonance NMR.

Yeast Two-Hybrid Assays. Gal4p activation domain (AD)−*URE2* fusion and Gal4p binding domain (BD)−*URE2* fusion constructs were cotransformed into strain AH109 (Clonetech) and selected for growth on synthetic complete medium lacking leucine and tryptophan (SC-Leu-Trp). Cotransformations were then serially diluted or streaked to single colonies on SC-Leu-Trp-His or SC-Leu-Trp-His-Ade media to test whether the various *URE2* constructs interact and activate the expression of the Gal4p-regulated reporter constructs (*ADE2* and *HIS3*). The vectors pGADT7-T and pGBKT7-53 (Clontech) encode Gal4p activation and binding domain fusions of SV40 large T-antigen and p53, respectively. An interaction between these proteins has previously been described and is used as a positive control in the two-hybrid assay for activation of the *HIS3*, *ADE2*, and *lacZ* reporter genes (44) As a negative control, the vector pGBKT7-lam (Clontech) encoding the human lamin C protein fused to the Gal4p binding domain was cotransformed with pGADT7-T. These proteins do not interact in the two-hybrid assay.

Activation of the *lacZ* reporter construct was tested by measuring β-galactosidase activity in extracts of AH109 cotransformants. In strain AH109, the *lacZ* reporter is under the control of the weak promoter of *MEL1*, the endogenous α-galactosidase of *S. cerevisiae*. To detect *lacZ* activity, we used the more sensitive substrate chlorophenol red-β-D-galactopyranoside (CPRG) rather than *o*-nitrophenol-β-D-galactopyranoside (ONPG). Briefly, cotransformants were grown in liquid SC-Leu-Trp to OD_{600} 0.5−0.8. Cultures were centrifuged for 30 s in a microcentrifuge and resuspended in buffer 1 (100 mM HEPES, 150 mM NaCl, 2 mM L-aspartate hemi-Mg salt, 10 mg/mL bovine serum albumin, 0.0005% Tween 20, pH 7.3). Cell extracts (0.1 mL) were prepared by freezing cultures in liquid nitrogen for 1 min followed by thawing for 1 min in a 37 °C water bath. Three freeze/thaw cycles were performed to ensure complete cell lysis. Enzyme assays were initiated by the addition of 0.7 mL of 2.2 mM CPRG in buffer 1. The *lacZ* activity is indicated by the hydrolysis of the substrate CPRG generating a yellow to red color change. After sufficient color development, enzyme assays were terminated by the addition of 0.5 mL of 3 M $ZnCl_2$, and the absorbance at 578 nm was recorded. β-Galactosidase activity is reported as Miller units where units are $1000 \times OD_{578}$ per minute per OD_{550} of cells.

[URE3] Induction. Strains YHE711 (*MATa ura2 leu2*) and MP174 (*MATa ura2 leu2 URE2::URE2Δ71−95* $P_{DAL5}CAN1$) were transformed with plasmids overexpressing either *URE2* (YEp351G-URE2) or *URE2Δ71−95* (YEp351G-*URE2Δ71-95*) under the control of the inducible *GAL1* promoter. Ten

transformants were mixed, resuspended in water, and plated on SGal (2%), raffinose (1%), −leucine dropout plates (SGal-Leu). Plates were incubated at 30 °C for 3 days and dilutions of 10^7, 10^6, 10^5, and 10^4 cells were plated onto synthetic dextrose medium with ureidosuccinate (USA) (33 μg/mL). Plates were incubated at 30 °C and USA$^+$ colonies were counted after 5 days.

Proteolytic Digests. Control experiments indicated that Ure2p65FX is completely digested into fragments consisting of residues 1−65 and 66−354 following incubation at room temperature with 2 units of recombinant factor Xa (Novagen) for 2 h. Digests were scaled up to 250 μL reactions containing 50 μg of Ure2p-65Fx and 2 U of recombinant factor Xa in buffer A (50 mM Tris, 100 mM NaCl, 5 mM CaCl$_2$, pH 8.0). Identical reactions that did not contain the protease were included as controls. After a 2 h incubation at room temperature, the protease was removed from the digestion by adding 250 μL of Xarrest agarose (Novagen) equilibrated in buffer A. The digest−slurry mix was added to a 2 mL spin column and incubated at room temperature for 5 min. The reactions were centrifuged at 1000*g* for 5 min to remove the cleaved protein from the captured protease. Following the removal of the protease, aliquots of the digestion were analyzed by SDS- and native-PAGE.

RESULTS

Two-Hybrid Analysis. To test for possible interaction of the Ure2p prion domain and nitrogen regulatory domain, we first used the yeast two-hybrid system. One protein fragment is fused to the activation domain of the Gal4p transcription factor, while the other fragment is fused to the Gal4p DNA-binding domain. Activation of *GAL* promoters is only observed if the two protein fragments interact, bringing together the parts of Gal4p (*29*). As previously reported (*19*), linkage of the full-length Ure2 protein or the C-terminal domain to the Gal4 binding domain produced activation even with the activation vector alone (Figure 1), indicating that the Ure2p C-terminal domain has activation activity.

With the prion domain (Ure2p$^{1-80}$) fused to the Gal4 DNA binding domain and the C-terminal domain (Ure2p$^{81-354}$) or the full-length Ure2p fused to the Gal4 activation domain, no interaction was observed, either as growth on selective media or as β-galactosidase activity above background levels (Figure 1).

Proteolytic Nicking Experiment. If the prion domain and nitrogen regulation domain interact, a nick between these regions might leave the two regions attached. We engineered a site for the factor Xa protease by inserting amino acids isoleucine and glutamic acid after Ure2p residue 63 producing IEGR, which is cleaved after the arginine (residue 65 of normal Ure2p). Cleavage of the purified enzyme by protease was complete, as judged by SDS polyacrylamide gel electrophoresis (Figure 2). Native polyacrylamide gel electrophoresis showed that the fragments produced did not comigrate, indicating that their mutual affinity was relatively low (Figure 2).

Surface Plasmon Resonance. A sensitive method to detect interactions between two components, surface plasmon resonance involves attaching one component to a surface and passing a solution of the other component over this surface. Interaction of the dissolved component with the attached component changes the refractive index in the immediate
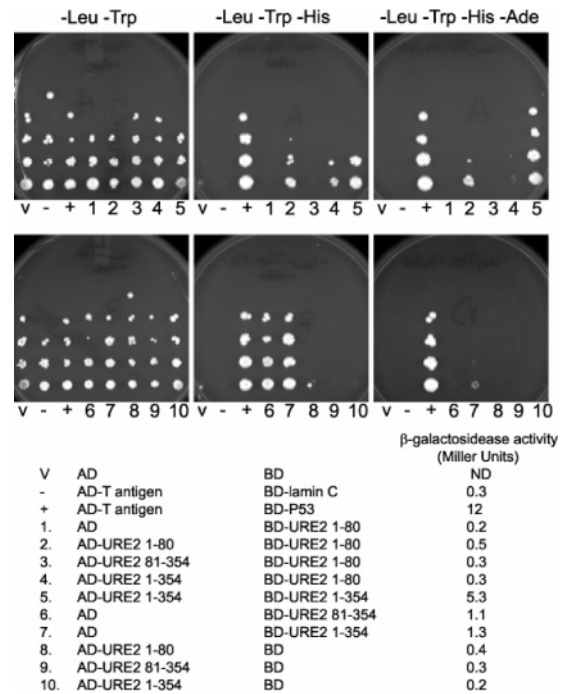

FIGURE 1: Two-hybrid analysis of prion domain and C-terminal domain of Ure2p. Plasmids with the indicated fusions to the Gal4p binding domain (BD, pGADT7) and activating domain (AD, pGBKT7) were tested for activation of Gal promoters in strain AH109 by growth of serial 10-fold dilutions (bottom to top) of cells on the indicated media. Interactions are also assayed as β-galactosidase (below). The interaction between the SV40 large T-antigen and murine p53 has previously been reported (*44*) and is used as a positive control for the activation of reporter gene expression. The absence of reporter gene activation between the noninteracting proteins human lamin C and SV40 large T-antigen is used as a negative control.
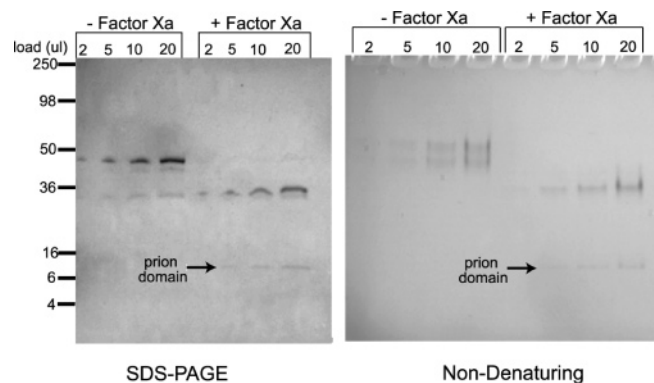

FIGURE 2: Proteolysis in the tether region frees the prion domain. Purified Ure2p with a factor X site between residues 65 and 66 was digested with factor X. Denaturing and nondenaturing polyacrylamide gel electropherograms are shown.

vicinity of the surface, and this change is detected. It was essential to fix the prion domain to the surface because it otherwise would readily form amyloid. Ure2p$^{1-80}$ with a C-terminal cysteine residue was constructed to enable the specific thioester coupling to a flat carboxylated surface in the nonaggregated form. The steric constraints of the surface immobilization in the absence of the customary flexible matrix can be expected to prohibit aggregation. Exposure of the surface-immobilized peptide with C-terminal fragments (81−354) at concentrations between 0.01 and 1 mg/mL generated signal offsets between 10 and 100 RU. However,
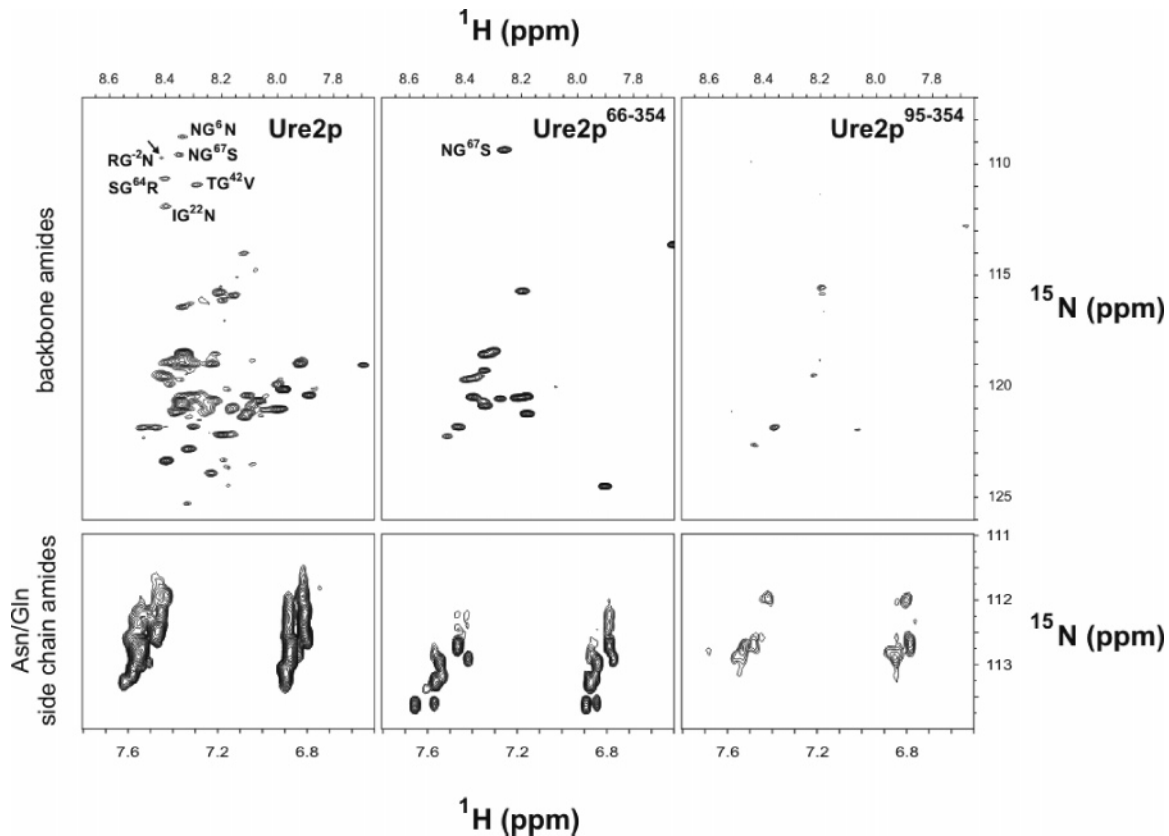
FIGURE 3: NMR analysis of Ure2p$^{1-354}$, Ure2p$^{66-354}$, and Ure2p$^{95-354}$. ^{15}N$-^1$H-HSQC spectra for the uniformly ^{15}N-enriched proteins were acquired at 600 MHz ^{1}H frequency. The upper panels show the backbone amide area of the spectra, where a considerable number (>70) of sharp peaks can be seen for the full-length protein, but far fewer for the constructs missing the N-terminal prion domain. Peaks that correspond to glycine residues are labeled with their tentative resonance assignments on the basis of their close proximity to ^{15}N shift values predicted for "random coil" residues when accounting for nearest neighbor effects (30). The arrow in the full-length Ure2p spectrum indicates the position of one weak glycine peak, just below the threshold level shown, and corresponds to Gly−2 in the N-terminal peptide preceding Ure2p. The lower panels show the area of asparagine and glutamine side chains of the same spectra. Whereas the full-length Ure2p shows a very strong signal for asparagine and glutamine side chains, the other constructs are markedly decreased.

the offsets were concentration-independent, indicating that they result from nonspecific hydrophobic interactions with the sensor surface that is imperfectly matched with the reference surface (data not shown). As a positive control, significant surface binding was observed with a polyclonal antibody to Ure2p. To examine a possible temperature dependence of the interaction by unfavorable entropic contributions at 25 °C, the binding experiments were repeated at 13 °C, but this again resulted in no detectable concentration-dependent binding.

NMR. Full-length Ure2p, Ure2p$^{66-354}$, and Ure2p$^{95-354}$ were examined by ^{1}H$-^{15}$N HSQC NMR (Figure 3). Under the conditions used, residues in unstructured parts of the molecule are subject to large-amplitude, rapid internal motions, which result in narrower, more intense resonance peaks. Residues in structured parts of large molecules (Ure2p is a homodimer of ∼82 kDa) are much less mobile and change their orientations relative to the magnetic field by a rate determined by the overall rotational diffusion of the homodimer. This results in rapid relaxation during the parts of the experiment that transfer magnetization from ^{1}H to ^{15}N and back. As a result, both the integrated and maximum intensities of the corresponding resonance peaks are vanishingly low and they are not detected above background. The observed peaks in the spectra (except the large peaks for the glutamine and asparagine side chains) are distributed in the "random coil region" for backbone amide hydrogens, H^N

(from 7.85 to 8.46 ppm), and are quite intense and sharp, indicating that the corresponding amino acid residues are highly flexible.

We find six peaks in the spectral region where glycine residues normally resonate (chemical shift for ^{15}N is around 110 ppm) in the full-length Ure2p (labeled in Figure 3). In the expressed protein, there is one glycine in the N-terminal tag, four glycine residues are found in Ure2p$^{1-65}$ and one (Gly67) in Ure2p$^{66-94}$. After correction of neighboring residue effects, their ^{15}N chemical shifts fall very close to values predicted for glycine residues in random coil regions (rmsd < 0.2 ppm) (30), allowing their tentative resonance assignment. The peak tentatively assigned to Gly−2 in the N-terminal tag (amino acids in the N-terminal tag are assigned negative values) is very weak and disappears completely upon saturation of the solvent signal (data not shown), indicating that it is subject to rapid hydrogen exchange. Rapid exchange is predicted for this residue due to base-catalyzed exchange induced by its preceding arginine residue (31), corroborating the chemical shift based assignment. We find one glycine peak in the Ure2p$^{66-354}$ spectrum and no peak for Ure2p$^{95-354}$. The position of the glycine resonance remaining in the Ure2p$^{66-354}$ spectrum coincides with that of Gly67 (NGS) in the full-length Ure2p spectrum, and its presence indicates that this region of the polypeptide chain is highly flexible.

There are some very sharp peaks at ^{15}N shifts around 125 ppm in all three spectra that are mostly of low integrated intensity. Such large ^{15}N shifts are commonly observed for C-terminal residues, but only one common C-terminal residue is expected for all three constructs and the observed peaks are at different positions in each of the spectra, making this interpretation less likely. We believe that these peaks correspond to small amounts of proteolytic cleavage products. For the Ure2p sample, the intensity of these resonances increased between the two HSQC spectra recorded sequentially, also pointing toward proteolysis. Indeed the prion domain of Ure2p is known to be highly sensitive to trace amounts of proteases (*15*, *21*). The resonance peaks for aspartic acid and glutamine side chains (^{15}N shift ∼112 ppm and NH shifts of 7.0 and 7.7 ppm) extensively overlap one another and therefore are very strong in Ure2p and weaker in Ure2p$^{66-354}$ and Ure2p$^{95-354}$, indicating that a large number of asparagine and glutamine residues are flexible in full-length Ure2p.

In total, we can count about 72 resolved backbone amide peaks upfield of 125 ppm in full-length Ure2p. Clearly, as a result of extensive overlap present in the spectrum, this is a lower limit for the total number of flexible residues in the protein. In an attempt to account for these buried peaks, we integrated the total intensity in this region and normalized it relative to the intensity of the resolved glycine residues. Using this procedure yields 103 ± 15 unstructured residues for full-length Ure2p and 21 ± 4 residues for Ure2p$^{66-354}$. Since only very few peaks are seen for Ure2p$^{95-354}$, the unstructured residues must be located almost entirely in the prion domain and tether regions of Ure2p (about 90 residues in all) and in the tag peptides (13 residues for full-length Ure2p and 12 residues for Ure2p$^{66-354}$).

The Tether. The data above suggest that there is no interaction of the prion domain of Ure2p with the C-terminal nitrogen regulation domain. How to explain the elevated prion formation on deletion of segments of the C-terminal domain? Conceivably, placement of the large C-terminal domain around the central amyloid core interferes physically with the assembly of filaments by the prion domain. This model would predict that deleting the part of Ure2p between the amyloid core (residues 1−65) and the structured C-terminal domain (residues 95−354) should adversely affect prion formation or propagation.

We therefore deleted Ure2p residues 71−95, a part of the protein that is part of neither the GST-like structure of the C-terminal nitrogen regulation domain nor the extremely protease-resistant *β*-sheet-rich amyloid core but connects these two domains in the prion form. *URE2Δ71−95* was both integrated at the normal *URE2* locus from the *URE2* promoter and expressed on a plasmid from the *GAL1* promoter (Table 1). Ure2pΔ71−95 was fully capable of being a prion and showed, if anything, increased ability to induce the prion form of Ure2p or Ure2pΔ71−95 (Table 1).

DISCUSSION

In all of the prion proteins studied to date, a restricted region forms the core of the amyloid structure and is necessary for the prion properties of the molecule, but mutations affecting prion generation are distributed through

Table 1: Effect of Deleting the Tether Region (71−95) on [URE3] Generation[a]

strain	plasmid	USA$^+$ colonies/10^6 cells
YHE711	YEp351G	41
YHE711	YEp351G-URE2	5 300
YHE711	YEp351G-URE2Δ71−95a	5 600
YHE711	YEp351G-URE2Δ71−95b	3 200
MP174	YEp351G	61
MP174	YEp351G-URE2	6 800
MP174	YEp351G-URE2Δ71−95a	19 000
MP174	YEp351G-URE2Δ71−95b	23 000

[a] Strain YHE711 (*MATa ura2 leu2*) and strain MP174 (*MATa ura2 leu2 URE2::URE2Δ71−95* P$_{DAL5}$*Can1*) were transformed with the indicated plasmids and plated on SD-Leu dropout media for 3−4 days. For each transformation, 10 colonies were selected, mixed in water, and spotted onto Sgal (2%), raffinose (1%) − leucine media. Plates were incubated at 30 °C, and dilutions were plated onto SD + USA. USA$^+$ colonies were counted after 5 days at 30 °C. Plasmids YEp351G-*URE2Δ71−95* a and b are two independent clones.

most of the molecule. For Ure2p, Sup35p, and HETs, deletion of the nonamyloid part of the molecule dramatically increases prion formation in vivo and amyloid formation in vitro (*5*, *6*, *12*, *14*, *17*). De novo prion generation has not yet been shown experimentally for the TSEs (but see ref *32*) but is presumed to be the basis for the "spontaneous" and inherited cases of Creutzfeldt−Jakob disease (CJD). The mutations producing inherited CJD are distributed throughout the PrP molecule and are not restricted to the part that acquires *β*-sheet structure in PrP-res (reviewed in ref *33*). These results have been interpreted to mean that parts of the molecule outside that forming the amyloid core interact with and thereby prevent the prion domain from converting to amyloid. However, previous studies have not determined whether there is an interaction between N-terminus and C-terminus of Ure2p (see introduction).

We have sought evidence of interaction of the N-terminal prion domain and the C-terminal regulatory domain by a variety of in vivo and in vitro methods. Our two-hybrid results show no evidence of interaction between Ure2p$^{1-80}$ and Ure2p$^{81-354}$. Likewise, surface plasmon resonance data indicates no interaction under the conditions used. Nicking the prion domain results in the release of the fragment N-terminal to the nick, again suggesting absence of interaction.

Our NMR studies argue that the prion domain is largely unstructured but do not rule out interaction of a few residues with the C-terminus. Comparison of the spectra for the different constructs clearly indicates that there are numerous highly flexible amino acids in Ure2p that are largely reduced in Ure2p$^{66-354}$ and basically missing in Ure2p$^{95-354}$. All glycine residues in residues 1−95 appear to be flexible. Counting individual peaks and estimating flexible residues by integrating total intensity likewise support the conclusion that most of this region is unstructured. However, it is difficult to give an exact border between the flexible and folded regions.

Our evidence that the Ure2p N-terminus is unstructured recalls the native unstructured character of several other amyloid-forming proteins, notably α-synuclein (*34*). Moreover, the amyloid core of the HETs protein is, like that of Ure2p, largely unstructured in its soluble form (*14*). The protease-resistant core of the amyloid form, residues 218−

289, overlaps only partially with the structured part of the soluble form, residues 1−227. Although the structure of the amyloid form of PrP (called PrP^{Sc} or PrP-res) is not clear, it seems to form in large part by conversion of the unstructured residues 90−120 of PrP to β-sheet form (*33*). Thus, it seems that the driving force for most prions is a change from an unstructured form to amyloid, rather than a change from helix to sheet, as it is often portrayed. The structured part of what may become amyloid provides the energy barrier to prion formation and propagation.

If the Ure2p prion domain does not interact with the C-terminal functional domain, how are we to explain the dramatic enhancement of prion formation on deleting parts of the C-terminal domain? Packing of the C-terminal domain around the amyloid core may restrict the formation of filaments, explaining this effect. However, even modest deletions of the C-terminus (eight amino acids), which have negligible influence on the mass of the C-terminal appendage, produce dramatic increases in prion formation (*12*). Moreover, we find that deletion of the tether region, Ure2p residues 71−95, produces no decrease in prion formation. If packing of C-termini were the factor restricting amyloid formation, deletion of the tether would be expected to enhance that effect.

Artificially connecting the two subunits to prevent monomerization of Ure2p is reported to prevent filament formation (*35*). Although there is no correlation with the location of the dimer interface, it is possible that the mutations in the C-terminus that elevate prion formation do so by destabilizing the dimer. Alternatively, the C-terminal domain may bind to another protein that interacts with the Ure2p prion domain. Ure2p is known to interact with Gln3p in its nitrogen regulation activity (*36−38*, reviewed in ref *39*), retaining Gln3p in the cytoplasm when a good nitrogen source is available but releasing it otherwise. However, [URE3] arises at the same frequency in cells grown on the good nitrogen source ammonia as on the poor nitrogen source proline. Chaperones play a prominent role in prion generation and propagation (*40*, *41*), including [URE3] (*42*, *43*). It is possible that mutations outside the Ure2p prion domain affect prion generation in part by altering the interactions of the protein with chaperones. Studies are underway to test these possibilities.

ACKNOWLEDGMENT

REFERENCES

1. Wickner, R. B. (1994) Evidence for a prion analog in *S. cerevisiae*: the [URE3] non-Mendelian genetic element as an altered *URE2* protein, *Science 264*, 566−569.
2. Coustou, V., Deleu, C., Saupe, S., and Begueret, J. (1997) The protein product of the *het-s* heterokaryon incompatibility gene of the fungus *Podospora anserina* behaves as a prion analog, *Proc. Natl. Acad. Sci. U.S.A. 94*, 9773−9778.
3. Paushkin, S. V., Kushnirov, V. V., Smirnov, V. N., and Ter-Avanesyan, M. D. (1997) In vitro propagation of the prion-like state of yeast Sup35 protein, *Science 277*, 381−383.
4. King, C.-Y., Tittmann, P., Gross, H., Gebert, R., Aebi, M., and Wuthrich, K. (1997) Prion-inducing domain 2-114 of yeast Sup35 protein transforms in vitro into amyloid-like filaments, *Proc. Natl. Acad. Sci. U.S.A. 94*, 6618−6622.
5. Glover, J. R., Kowal, A. S., Shirmer, E. C., Patino, M. M., Liu, J.-J., and Lindquist, S. (1997) Self-seeded fibers formed by Sup35, the protein determinant of [*PSI+*], a heritable prion-like factor of S. cerevisiae, *Cell 89*, 811−819.
6. Taylor, K. L., Cheng, N., Williams, R. W., Steven, A. C., and Wickner, R. B. (1999) Prion domain initiation of amyloid formation in vitro from native Ure2p, *Science 283*, 1339−1343.
7. Speransky, V., Taylor, K. L., Edskes, H. K., Wickner, R. B., and Steven, A. (2001) Prion filament networks in [URE3] cells of *Saccharomyces cerevisiae*, *J. Cell. Biol. 153*, 1327−1335.
8. Dos Reis, S., Coulary-Salin, B., Forge, V., Lascu, I., Begueret, J., and Saupe, S. J. (2002) The HET-s prion protein of the filamentous fungus Podospora anserina aggregates in vitro into amyloid-like fibrils, *J. Biol. Chem. 277*, 5703−5706.
9. Maddelein, M. L., Dos Reis, S., Duvezin-Caubet, S., Coulary-Salin, B., and Saupe, S. J. (2002) Amyloid aggregates of the HET-s prion protein are infectious, *Proc. Natl. Acad. Sci. U.S.A. 99*, 7402−7407.
10. Wickner, R. B., Liebman, S. W., and Saupe, S. (2004) Prions of yeast and filamentous fungi, in *Prion Biology and Diseases* (Prusiner, S. B., Ed.) in press, Cold Spring Harbor Laboratory Press, Cold Spring Harbor, NY.
11. TerAvanesyan, A., Dagkesamanskaya, A. R., Kushnirov, V. V., and Smirnov, V. N. (1994) The *SUP35* omnipotent suppressor gene is involved in the maintenance of the non-Mendelian determinant [psi+] in the yeast *Saccharomyces cerevisiae*, *Genetics 137*, 671−676.
12. Masison, D. C., and Wickner, R. B. (1995) The *SUP35* omnipotent suppressor gene is involved in the maintenance of the non-Mendelian determinant [psi+] in the yeast *Saccharomyces cerevisiae*, *Science 270*, 93−95.
13. Derkatch, I. L., Chernoff, Y. O., Kushnirov, V. V., Inge-Vechtomov, S. G., and Liebman, S. W. (1996) Genesis and variability of [*PSI*] prion factors in *Saccharomyces cerevisiae*, *Genetics 144*, 1375−1386.
14. Balguerie, A., Dos Reis, S., Ritter, C., Chaignepain, S., Coulary-Salin, B., Forge, V., Bathany, K., Lascu, I., Schmitter, J.-M., Riek, R., and Saupe, S. (2003) Domain organization and structure−function relationship of the HET-s prion protein of *Podospora anserina*, *EMBO J. 22*, 2071−2081.
15. Baxa, U., Taylor, K. L., Wall, J. S., Simon, M. N., Cheng, N., Wickner, R. B., and Steven, A. (2003) Architecture of Ure2p prion filaments: the N-terminal domain forms a central core fiber, *J. Biol. Chem. 278*, 43717−43727.
16. Masison, D. C., Maddelein, M.-L., and Wickner, R. B. (1997) The prion model for [URE3] of yeast: spontaneous generation and requirements for propagation, *Proc. Natl. Acad. Sci. U.S.A. 94*, 12503−12508.
17. Kochneva-Pervukhova, N. V., Poznyakovski, A. I., Smirnov, V. N., and Ter-Avanesyan, M. D. (1998) C-terminal truncation of the Sup35 protein increases the frequency of de novo gneration of a prion-based [*PSI*+] determinant in *Saccharomyces cerevisiae*, *Curr. Genet. 34*, 146−151.
18. Deleu, C., Clave, C., and Begueret, J. (1993) A single amino acid difference is sufficient to elicit vegetative incompatibility in the fungus *Podospora anserina*, *Genetics 135*, 45−52.
19. Fernandez-Bellot, E., Guillemet, E., Baudin-Baillieu, A., Gaumer, S., Komar, A. A., and Cullin, C. (1999) Characterization of the interaction domains of Ure2p, a prion-like protein of yeast, *Biochem. J. 338*, 403−407.
20. Kulkarni, A. A., Abul-Hamd, A. T., Rai, R., El Berry, H., and Cooper, T. G. (2001) Gln3p nuclear localization and interaction with Ure2p in *Saccharomyces cerevisiae*, *J. Biol. Chem. 276*, 32136−32144.
21. Thual, C., Bousset, L., Komar, A. A., Walter, S., Buchner, J., Cullin, C., and Melki, R. (2001) Stability, folding, dimerization, and assembly properties of the yeast prion Ure2p, *Biochemistry 40*, 1764−1773.
22. Perrett, S., Freeman, S. J., Butler, P. J. G., and Fersht, A. R. (1999) Equilibrium folding properties of the yeast prion protein determinant Ure2, *J. Mol. Biol. 290*, 331−345.
23. Baxa, U., Ross, P. D., Wickner, R. B., and Steven, A. C. (2004) The N-terminal prion domain of Ure2p converts from an unfolded to a thermally resistant conformation, *J. Mol. Biol. 339*, 259−264.
24. (a) Komar, A. A., Guillemet, E., Reiss, C., and Cullin, C. (1998) Enhanced expression of the yeast Ure2 protein in *Escherichia*

coli: the effect of synonymous codon substitutions at a selected place in the gene, *Biol. Chem. 379*, 1295−1300. (b) Edskes, H. K., and Wickner, R. B. (2002) Conservation of a portion of the *S. cerevisiae* Ure2p prion domain that interacts with the full − length protein, *Proc. Natl. Acad. Sci. U.S.A. 99* (Suppl. 4), 16384−16391.

25. Schuck, P., Boyd, L. F., and Andersen, P. S. (1999) Measuring protein interactions by optical biosenors, in *Current Protocols in Protein Science* (Coligan, J. E., Dunn, B. M., Speicher, D. W., and Wingfield, P. T., Eds.) pp 20.2.1−20.2.21, John Wiley & Sons, New York.

26. Margulies, D. H., Corr, M., Boyd, L. F., and Khilko, S. N. (1993) MHC class I/peptide interactions: binding specificity and kinetics, *J. Mol. Recognit. 6*, 59−69.

27. Kay, L. E., Keifer, P., and Saarinen, T. (1992) Pure absorption gradient enhanced heteronuclear single quantum correlation spectroscopy with improved sensitivity, *J. Am. Chem. Soc. 114*, 10663−10665.

28. Delaglio, F., Grzesiek, S., Vuister, G. W., Zhu, G., Pfeifer, J., and Bax, A. (1995) NMRPipe: a multidimensional spectral processing system based on Unix pipes, *J. Biomol. NMR 6*, 277−293.

29. Fields, S., and Sternglanz, R. (1994) The two-hybrid system: an assay for protein−protein interactions, *Trends Genet. 10*, 286−292.

30. Wang, Y. J., and Jardetzky, O. (2002) Investigation of the neighboring residue effects on protein chemical shifts, *J. Am. Chem. Soc. 124*, 14075−14084.

31. Bai, Y., Milne, J. S., and Englander, S. W. (1994) Primary structure effects on peptide group exchange. Primary structure effects on peptide group exchange, *Proteins 17*, 75−86.

32. Legname, G., Baskakov, I. V., Nguyen, H.-O. B., Reisner, D., Cohen, F. E., DeArmond, S. J., and Prusiner, S. B. (2004) Synthetic mammalian prions, *Science 305*, 673−676.

33. Riesner, D. (2003) Biochemistry and structure of PrPC and PrPSc, *Br. Med. Bull. 66*, 21−33.

34. Weinreb, P. H., Zhen, W., Poon, A. W., Conway, K. A., and Lansbury, P. T. (1996) NACP, a protein implicated in Alzheimer's diseases and learning, is natively unfolded, *Biochemistry 35*, 13709−13715.

35. Bousset, L., Thomson, N. H., Radford, S. E., and Melki, R. (2002) The yeast prion Ure2p retains its native a-helical conformation upon assembly into protein fibrils in vitro, *EMBO J. 21*, 2903−2911.

36. Blinder, D., Coschigano, P. W., and Magasanik, B. (1996) Interaction of the GATA factor Gln3p with the nitrogen regulator Ure2p in *Saccharomyces cerevisiae*, *J. Bacteriol. 178*, 4734−4736.

37. Beck, T., and Hall, M. N. (1999) The TOR signaling pathway controls nuclear localization of nutrient-regulated transcription factors, *Nature 402*, 689−692.

38. Hardwick, J. S., Kuruvilla, F. G., Tong, J. K., Shamji, A. F., and Schreiber, S. L. (1999) Rapamycin-modulated transcription defines the subset of nutrient-sensitive signaling pathways directly controlled by the tor proteins, *Proc. Natl. Acad. Sci. U.S.A. 96*, 14866−14870.

39. Cooper, T. G. (2002) Transmitting the signal of excess nitrogen in *Saccharomyces cerevisiae* from the Tor proteins to th GATA factors: connecting the dots, *FEMS Microbiol. Rev. 26*, 223−238.

40. Chernoff, Y. O., Lindquist, S. L., Ono, B.-I., Inge-Vechtomov, S. G., and Liebman, S. W. (1995) Role of the chaperone protein Hsp104 in propagation of the yeast prion-like factor [psi⁺], *Science 268*, 880−884.

41. Jung, G., Jones, G., Wegrzyn, R. D., and Masison, D. C. (2000) A role for cytosolic Hsp70 in yeast [PSI+] prion propagation and [PSI+] as a cellular stress, *Genetics 156*, 559−570.

42. Moriyama, H., Edskes, H. K., and Wickner, R. B. (2000) [URE3] prion propagation in *Saccharomyces cerevisiae*: requirement for chaperone Hsp104 and curing by overexpressed chaperone Ydj1p, *Mol. Cell. Biol. 20*, 8916−8922.

43. Roberts, B. T., Moriyama, H., and Wickner, R. B. (2003) [URE3] prion propagation is abolished by a mutation of the primary cytosolic Hsp70 of budding yeast, *Yeast 21*, 107−117.

44. Li, B., and Fields, S. (1993) Identification of mutations in p53 that affect its binding to SV40 T antigen by using the yeast two-hybrid system, *FASEB J. 7*, 957−963.